Degfie *et al. Applied Biological Chemistry* (2022) 65:76
https://doi.org/10.1186/s13765-022-00740-8

KSABC
The Korean Society for Applied Biological Chemistry

ARTICLE

Open Access

In vitro antibacterial, antioxidant activities, molecular docking, and ADMET analysis of phytochemicals from roots of *Hydnora johannis*

Teshome Degfie[1], Milkyas Endale[1*], Tarekegn Tafese[1], Aman Dekebo[1,2*] and Kebede Shenkute[1]

Abstract

Hydnora johannis is a medicinal plant traditionally used to treat various ailments. Chemical investigation of the dichloromethane (DCM)/methanol (MeOH) (1:1) roots extract of *Hydnora johannis* afforded three compounds (**1–3**), reported herein for the first time from the species. The structures of the isolated compounds **1–3** were elucidated using 1D and 2D NMR spectroscopic analysis and comparison with literature data. The highest zone of inhibition value was measured for DCM/MeOH extract (10.75 ± 0.25 mm) against *Staphylococcus aureus* at concentration of 0.25 mg/mL, promising in comparison to the standard amoxicillin (16.0 ± 0.0 mm, 0.25 mg/mL). At concentration of 0.25 mg/mL, the largest mean inhibition zone of 12.0 ± 0.0 mm was measured for compound **2** against *Pseudomonas aeruginosa*, comparable to the standard drug amoxicillin (16.0 ± 0.0 mm, 0.25 mg/mL). Compound **2** displayed better binding affinity with minimum binding energy of − 8.7 kcal/mol (PqsA), − 7.6 kcal/mol (DNA gyrase), and − 7.4 kcal/mol (*S aureus* PK) than amoxicillin (− 7.3, − 6.1, and − 7.0 kcal/mol, respectively). This suggests that compound **2** may act as potential inhibitor of the tested bacterial proteins. Compound **1** satisfies the Lipinski's rule of five with zero violations. Compound **2** obey the MW (452.4 g/mol) and iLogP (< 5) rules, and compound **3** obey the NHD (4) and NHA (6) rules. Compounds **2** recorded iLogP value less enough than five (1.55), implying its optimal lipophilicity. Compounds **1** and **3** satisfy the veber's rule (NRB < 12, and TPSA < 140 unit). Compound **2** and **3** exhibited negligible acute toxicity (LD_{50} > 5000, Toxicity class > 5. Compound **2** demonstrated maximum scavenging activity (67.87%) with IC_{50} value of 0.190 µg/mL, compared to ascorbic acid (78.21%) with IC_{50} value of 0.014 µg/mL at concentration of 12.5 µg/mL. Overall, the in vitro antibacterial activity of the extracts and compounds, molecular docking analysis and radical scavenging activity results of the isolated compounds suggest DCM/MeOH crude extract and compound **2** are promising antibacterial agents whereas compound **2** and **3** are promising antioxidants which corroborates with the traditional uses of the roots of *H. johannis*.

Keywords: Antibacterial, Molecular docking, Antioxidant, *Hydnora johannis*

Introduction

The genus *Hydnora* (Hydnoraceae) includes approximately eight taxonomically identified species [1], the only known angiosperm with no leaves or scales of any sort [2, 3], all are chiefly hypogenous, root-parasitic herbs, with an extremely reduced vegetative body (Additional file 1: Fig. S13), which has no leaves or bracts and consists of a massive, fleshy horizontal rhizome like root covered

*Correspondence: milkyas.endale@astu.edu.et; amandekeb@gmail.com

[1] Department of Applied Chemistry, Adama Science and Technology University, P.O. Box 1888, Adama, Ethiopia
[2] Institute of Pharmaceutical Sciences, Adama Science and Technology University, P.O. Box 1888, Adama, Ethiopia

with haustoria roots as wart like outgrowth [1, 2]. Members of this genus have long been used in folk medicine to treat various ailments, such as diarrhea, cholera, hemorrhoid, swollen abdomen, lung cancer, breast cancer, and diabetic [4, 5]. Phytochemical constituents of genus *Hydnora* include flavonoids, tannins, terpenoids, saponins, alkaloids, and essential oils [6, 7]. These compounds exhibit diverse bioactivities, including antioxidant, antibacterial, antifungal, hepatoprotective, and anticancer [8]. *Hydnora johannis* Becc is a subterranean holoparasitic (non-photosynthetic) herb with often massive root systems spreading laterally from the host. It is an obligate root parasite found on *Acacia* and *Albiziz* species as well as *Kigelia africana*; growing between 1000 and 1500 m altitudes [1]. It is widely distributed in Ethiopia, Eritrea, Somalia, Kenya, Tanzania, Rwanda and Democratic republic of Congo [2, 9]. In Ethiopia, it is identified by vernacular name Licce, Like, Likke, Lipti (Som), Dech-Merech (Oro), and available in different part of the country including Shewa, Sidamo, Bale, Arsi and Hararge, [10, 11]. Various traditional uses of the plant have been reported in Ethiopia, including treating breast cancer, lung cancer, diarrhea, hemorrhage, wound and painful body swelling, locally called GOFLA (Oromo language) around Erer Valley of Babile Wereda, Eastern Ethiopia [10–12]. Despite the widespread ethnomedicinal uses of this plant for ailments of various diseases, there exists no detailed study reports on the phytochemical analysis and pharmacological properties of *H. johannis*. Hence, reported herein are the molecular docking analysis (for the first time), antibacterial, antioxidant, and isolation of three compounds from the root of dichloromethane/methanol (1:1) extract of *H. johannis.*

Experimental part

General experimental procedure

The NMR spectra were recorded on Bruker Avance 400 MHz spectrometer with deuterated chloroform and methanol using TMS as internal standard. Analytical TLC plates with silica gel 60 F254 TLC (Merck, Germany) were used to determine TLC profiles. The spots on TLC plates were visualized using a UV lamp (254 and 365 nm). Silica gel column chromatography was performed at silica gel (60–120 mesh). All chemicals, solvents and reagents were used to analytical grade level.

Plant material collection and identification

The roots of *H. johannis* were collected from the district of Huruta town, Lode Hetosa Woreda, Arsi Zone, Oromia, Ethiopia, in September 2019. The plant material was authenticated by Melaku Wendafrash (Chief Technician, Botanist), and voucher specimen (TCY010) was deposited at the National Herbarium, Department of Biology, Addis Ababa University, Ethiopia.

Extraction and isolation of compounds from the roots of *H. johannis*

The powdered roots of *H. johanns* (500 g) were extracted with *n*-hexane for 72 h, three times at room temperature to obtain 18.3 g crude extract. The marc was further extracted with dichloromethane (DCM)/methanol (MeOH) (1:1), and MeOH (100%). The filtrates were concentrated in vacuum a rotary evaporator at 40ºC to obtain 30.6 g, and 24 g of crude extracts, respectively.

The DCM/MeOH (1:1) root extract (10 g) was subjected to silica gel column chromatography (silica gel 180 g) and eluted with increasing gradient of *n*-hexane/EtOAc followed by dichloromethane/methanol mixtures. A total of 119 fractions were collected (each 50 mL). Compound **1** (58 mg) was obtained from fraction 27-31using *n*-hexane/EtOAc (7:3) as eluent. Fractions 100–105 obtained with DCM/MeOH (7:3) were combined and purified using isocratic elution with 5% MeOH in DCM as eluent to afforded compound **2**, (57 mg) and compound **3**, (20 mg).

Antibacterial activity

Isolated compounds **2** and **3**, and *n*-hexane, DCM/MeOH (1:1), and MeOH extracts were studied for *in-vitro* antibacterial activity against four standard human bacterial pathogens; namely, *Staphylococcus aureus* (*S. aureus*, ATCC 25,923), *Escherichia coli* (*E. coli*, ATCC 25,922), *Pseudomonas aeruginosa* (*P. aeruginosa*, ATCC 27,853) and *Streptococcus pyogen (S. pyogen* ATCC19615) collected from Ethiopian Public Health Institute (EPHI). Experiments were done at the microbiology laboratory of the Applied Biology Department, Adama Science and Technology University, in collaboration with microbiologists. The degree of susceptibility of each bacterial strain to the isolated compounds was evaluated by using the agar medium disc-diffusion technique as per the standard protocols of Clinical and Laboratory Standards Institute (CLSI) [13]. That is, about 2–4 fresh colonies with similar morphology of each bacterial species were aseptically transferred into a saline solution using a sterile inoculating loop, and bacterial turbidity was adjusted in reference to 0.5 McFarland standard solution (10^8 CFU/mL). The Mueller Hinton Agar (HiMedia) medium was prepared as per the manufacturer's instruction. The bacterial suspension was then streaked by swapping with cotton swap onto Petri plates containing the medium. A sterilized Whatman No. 1 filter paper discs (6 mm in diameter) were prepared using a puncher to hold samples. A stock solution of each isolated compound (5 mg in 5 mL) was prepared in 4% DMSO. Thereafter, different

solutions, 1.00 mg/mL, 0.5 mg/mL and 0.25 mg/mL of each extract, and 0.5 mg/mL and 0.25 mg/mL of each compound (**2** and **3**) were prepared from their corresponding stock solutions. Standard antibiotic disc of Amoxicillin (0.25 mg/mL) and DMSO were served as positive and negative controls, respectively. Each solution of 100 µL was loaded onto separate paper discs (6 mm in diameter), placed discs onto the Petri plates with the bacterial culture inoculated MHA, and incubated at 37 °C for 18–24 h. Inhibition zones were monitored by the paper disc's clear area and measured by a caliper (in mm) [13, 14]. The experiment was done in duplicate aseptically, and the result was expressed as mean ± standard deviation using statistical analysis software of SPSS (version 20).

Molecular docking studies of the isolated compounds

In this study, the isolated compounds **1**–**3** were docked with proteins *E. coli* DNA gyrase B (PDB ID: 6F86), PqsA (PDB ID: 3T07) and *S. aureus* Pyruvate Kinase (PK) (PDB ID: 5OE3) as target proteins. AutoDock Vina 4.2 (MGL tools 1.5.7) was used to perform the molecular docking analysis to predict the potential binding modes of the test compounds with the target bacterial proteins [15]. The docking calculation results include binding energy (kcal/mol), hydrogen bond distances, and pictorial representation of viable docked poses. Chem Office tools (ChemDraw 16.0) was used to draw the structures of the compounds **(1–3)** with appropriate 2D orientations. Minimized energy of the compounds/ligands were obtained using ChemDraw3D ultra. The energy minimized ligand molecules were then used as input for AutoDock Vina to carry out the docking simulation.

Crystal structures of the receptor protein molecules were obtained from the protein data bank (PDB). The coordinates of the structures were complexed with water molecules and other atoms which are responsible for increased resolution. The proteins were prepared using protein preparation protocol [16], applying default parameters. The target protein file was generated by leaving the associated residue (remove water molecules and cofactors) with protein by using Auto Preparation of target protein file AutoDock 4.2 (MGL tools1.5.7). The grid box for docking simulation with size of $50 \times 50 \times 54$ Å points with a grid spacing of 0.375 Å was adjusted using the graphic user interface program in such a way that it surrounds the region of interest in the macromolecule. The potential binding energy between ligand and protein was obtained using the docking algorism provided by AutoDock Vina. The conformations with the most favorable (least) binding energy between the target proteins and compounds were selected for analyzing the interactions between the target receptor and ligands by Discovery studio visualizer and PyMOL. The ligands are represented in different colors, H-bonds and the interacting residues are represented in stick model representation.

In Silico pharmacokinetic analysis

Pharmacokinetic parameters were evaluated for the isolated compounds to investigate their drug candidate chances. The ADMET properties were evaluated with the aid of SwissADME, an online ADME prediction tool [17]. The drug-likeness of the compounds were predicted by adopting the Lipinski's Rule of five [18]. Structure of the isolated compounds (**1**–**3**) were converted to their canonical simplified molecular-input line-entry system (SMILE) and submitted to SwissADME and PreADMET tool to estimate in-silico pharmacokinetic parameters [17]. The toxicity profile of the studied compound (**1**–**3**) was predicted using ProTox-II Web tool [19]. The selection of the compounds as drug candidates was determined by a parameter called drug score. The higher the drug score value, the higher the compound's chance is considered a drug candidate [20].

Radical scavenging activity

The antioxidant activity of each of the isolated compounds from the root of *H. johannis* was evaluated based on the scavenging activity of the stable 2,2-diphenyl-1-picrylhydrazyl (DPPH) free radical [21]. Each sample was separately dissolved in methanol and serially diluted to give 200, 100, 50, and 25 µg/mL concentrations. Freshly prepared 0.04% DPPH solution in methanol was added to each concentration. The mixture was shaken and incubated in an oven at 37°C for 30 min. The absorbance of the resultant solution was measured at 517 nm using UV-Vis spectrophotometry. Ascorbic acid with a similar concentration of test sample was used as the positive control. The DPPH radical scavenging activity of each of the tested compounds was reported by percentage inhibition using the following formula:

$$\%DPPH\ inhibition = \frac{(A_{control} - A_{sample})}{A_{control}} \times 100\%$$

where $A_{control}$ is the absorbance of DPPH solution and $A_{sample}$is the absorbance of the test sample (DPPH solution plus compound) [21]. The DPPH radical scavenging activity of the compounds was also expressed as IC_{50}, the concentration of the test compound to give a 50% decrease of the absorbance from that of the control solution.

Results and discussion

The DCM/MeOH (1:1) root extracts of *H. johannis* was subjected to gravity column chromatography over silica gel to afford three compounds (**1–3**) (Fig. 1), reported

from this plant for the first time. The structures of each of the isolated compounds were elucidated by different spectroscopic techniques and comparison of their spectroscopic data to those previously reported in the literature. Compound **1** was isolated as a yellowish solid. The melting point of the compound was found to be in the range of 134 to 136ºC [22]. The TLC profile showed R_f value of 0.52 with *n*-hexane/EtOAc (7/3) mobile phase. The ^{1}H NMR (400 MHz, $CDCl_3$) spectrum displayed signals of olefinic protons at δ 5.33 (m, H6), methine proton signal at δ 3.51 (H3) assignable to an sp^3 oxygenated methine proton (Table 1, Additional file 1: Fig. S1).The ^{1}H NMR also showed proton signals at δ 2.00 (m, 2 H, H7), 2.33 (m, 2 H, H4) attributed to methylene and methine protons, respectively, and six methyl protons at 0.99 (H19), δ 0.87 (H21), 0.85 (H26), 0.81 (H27), 0.76 (H29), and 0.67 (H18). The remaining proton signals overlapped in the range of δ 1.26 to 2.00. The ^{13}C NMR (100 MHz, $CDCl_3$) spectrum displayed 29 carbon signals including two olefinic carbon signals at δ 140.8 (C5), 121.8 (C6), of which the former is sp^2 quaternary carbon, one sp^3methine at δ 71.9 (C3), two sp^3 quaternary carbons at δ 36.6 (C10) and 42.4 (C13), seven methine signals at δ 32.0 (C8), 50.2 (C9), 56.8 (C14), 56.1 (C17), 36.2 (C20), 45.9 (C24) and 29.2 (C25), six methyl carbons at δ 19.9 (C26), 19.5 (C27), 19.1 (C19), 18.8 (C21), 12.1 (C29) and 11.9 (C18), and eleven methylene carbon signals [δ 21.2 (C11), 23.1 (C28), 24.4 (C15), 26.1 (C23), 28.3 (C16), 31.6 (C2), 32.0 (C7), 34.1 (C22), 37.3 (C1), 39.8 (C12), 42.2 (C4)] (Table 1, Additional file 1: Figs. S2 and S3). The obtained ^{1}H/^{13}C NMR spectral data are found to be consistent with reported literature data of *β*-sitosterol, Figs. 1, [23, 24] reported herein for the first time from roots of *H. johannis*.

Compound **2**, was obtained as a brown solid. The TLC profile showed R_f value of 0.47 with DCM/MeOH (9/1) mobile phase. The ^{1}H NMR spectrum revealed the presence aromatic protons at δ 6.86 (d, *J* = 1.9 Hz, 1H, H2'), δ 6.78 (d, *J* = 8.1 Hz, 1H, H5') and δ 6.73 (dd, *J* = 8.1, 1.9 Hz, 1H, H6') with AMX spin system (ring B), and at δ 5.95 (d, *J* = 2.3 Hz, 1H, H6) and δ 5.87 (d, *J* = 2.3 Hz 1H, H8) assignable to AX type system (ring A) (Additional file 1: Table S-1; Fig. S4). The protons signals at δ 4.58 (d, *J* = 7.5 Hz, 1H, H2)/3.94 (m, 1H, H3), and at 2.87 (dd, *J* = 16.1, 5.5 Hz, 1H, H4a)/2.52 (dd, *J* = 16.1, 5.5 Hz, 1H, H4b) were assignable to methine and methylene protons of ring C, respectively. The ^{1}H NMR also displayed proton signals assignable to sugar moiety at δ 4.31 (d, *J* = 7.7 Hz, 1H, H1"), and ranging δ 3.21 to 3.71 (6H, H2" to H6") (Table 2). The ^{13}C NMR (100 MHz, CD_3OD) spectra displayed **2**1 well resolved carbon peaks. The peaks at δ 157.6 (C5), 157.4 (C7), 156.7 (C9), 146.1 (C3'), 146.0 (C4'), 132.1 (C1') and 100.7 (C10), are attributed to aromatic quaternary carbons of ring A and B of the flavan moiety (Additional file 1: Table S-1; Fig. S5 and S6). The carbon signals at δ 96.2 (C6), 94.5 (C8), 115.2 (C2'), 116.1 (C5') and 120.0 (C6') are in agreement with aromatic methine signals of ring A and B. The DEPT-135 spectrum (Additional file 1: Fig. S6) displayed methine and methylene carbons but no methyl carbon. The carbon methine carbon signals at δ 82.6 and 68.6, and methylene signals at δ 28.3 (C4) attributed to the oxy-methine (C2 and C3, respectively) and methylene (C4) of ring C of the flavan moiety. Furthermore, the ^{13}C spectrum revealed characteristic sugar peaks at δ 104 (C1"), 75.0 (C2"), 77.9 (C3"), 72.0 (C4"), 77.7 (C5"), and 61.6 (C1"). The methylene absorption at δ 61.6 suggests the sugar to be glucopyranose group. The linkages and substitution patterns were established from the COSY and HMBC analyses (Additional file 1: Table S-1; Figs. S7–S9). The HMBC spectrum displayed ^3J correlations between proton at δ 4.31 (H1")

Table 1 ^{1}H, ^{13}C NMR spectral data of compound **1**

Compound 1			^{13}C [23]
Position	^{1}H	^{13}C	
1		37.3	37.2
2		31.6	31.6
3	3.51 (m, 1 H)	71.9	71.8
4	2.33 (m, 1 H)	42.2	42.3
5		140.8	140.7
6	5.33 (m, 1 H)	121.8	121.7
7	2.00 (d, *J* = 7.0 Hz, 2 H)	32.0	31.9
8		32.0	31.9
9		50.2	50.1
10		36.6	36.5
11		22.8	21.1
12		39.8	39.8
13		42.4	42.3
14		56.8	56.7
15		24.4	24.3
16		28.3	28.2
17		56.1	56.0
18	0.67 (s, 3 H)	11.9	11.8
19	0.99 (s, 3 H)	19.1	19.4
20		36.2	36.1
21	0.87 (d, *J* = 6.9 Hz, 3 H)	18.8	18.8
22		34.1	33.9
23		26.1	26.1
24		45.9	45.8
25		29.2	29.1
26	0.85 (d, *J* = 6.9 Hz, 3 H)	19.9	19.8
27	0.81 (d, *J* = 7.2 Hz, 3 H)	19.5	19.0
28		23.1	23.1
29	0.76 (m, 3 H)	12.1	12.0

Table 2 ^{1}H, ^{13}C NMR spectral data of compound **3**

position	Comppund 3		^{13}C [26]	Position	Compound 3		^{13}C [26]
	^{1}H	^{13}C			^{1}H	^{13}C	
1	1.89 (m)	37.0	36.7	19	1.14 (s)	19.5	19.4
2	1.37 (m)	29.4	29.2	20		35.9	35.4
3	3.59 (m, 1 H)	78.9	76.8	21	0.81 (d)	18.5	18.5
4	2.31 (dd)	39.5	39.2	22	1.18 (m)	33.7	33.2
5		140.7	140.4	23	1.16 (m)	25.7	25.3
6	5.25 (bs, 1 H)	121.7	121.2	24		45.6	45.1
7	1.94 (s)	31.7	31.3	25	1.50 (m)	28.8	28.6
8	1.48 (m)	31.6	31.2	26	0.73 (d)	19.0	19.6
9	0.89 (m)	49.9	49.5	27	0.71 (d)	18.7	18.8
10		36.5	36.1	28	1.37 (m)	22.8	22.1
11	1.48 (m)	20.8	20.5	29	0.89 (m)	11.6	11.7
12	1.15 (m)	38.4	38.2	1′	4.42 (d)	100.8	100.7
13		42.3	41.8	2′	3.20 (m)	73.3	73.4
14	1.04 (m)	56.5	56.1	3′	3.31 (m)	75.5	76.8
15		24.0	23.8	4′	3.30 (m)	69.8	70.0
16	1.75 (m)	28.0	27.7	5′	3.46 (m)	76.1	76.7
17	1.13 (m)	55.8	55.3	6′	3.71 (m)	61.4	62.8
18	0.80 (s)	11.5	11.6				

with 96.2 (C6) and proton 5.87 (H8) with 104.1 (C1") suggests the attachment of the glucopyranose moiety to C7 of ring A. The spectral data of compound **2** obtained in this study is found to be in good agreement with reported data of catechine-7-O-glucoside [25]. Thus, based on the reported spectral data and the data from literature [25], compound **2** is identified to be flavan-3-ol-7-*O*-glucoside (catechine-7-*O*-glucoside, Fig. 1), reported herein for the first time from roots of *H. johannis*.

Compound **3** was obtained as a pale brown solid. The TLC profile showed R_f value of 0.56 with DCM/MeOH (9/1) mobile phase. The ^{1}H NMR (400 MHz, CD_3OD) spectrum displayed signals assignable to olefinic protons at δ 5.25 (H6), oxygenated methine proton at δ 4.29 (H3), methylene protons at δ 2.31 (dd, 2 H, H4), and six methyl protons at δ 1.14 (H19), 0.89 (H29), 0.81 (H21), 0.80 (H18), 0.73 (H26), and 0.71 (H27) (Table 2, Additional file 1: Fig. S10). The proton signals observed in the range of 3.12 to 4.29 were assignable to sugar moiety. The remaining proton signals overlapped in the range of δ 1.26 to 2.00. The ^{13}C NMR (100 MHz, $CDCl_3$) spectrum displayed 35 carbon signals including olefinic carbon at δ 140.7 (C5) and 121.7 (C6), of which the former suggest sp^2 quaternary carbon, sp^3oxy-carbon at δ 78.9 (C3), two sp^3 quaternary carbons at δ 36.5 (C10) and 42.3 (C13), and methine carbons at δ 31.6 (C8), 49.9 (C9), 56.5 (C14), 55.8 (C17), 35.9 (C20), 45.6 (C24) and 28.8 (C25), six methyl carbons at δ 19.5 (C19), 19.0 (C26), 18.7 (C27), 18.5 (C21), 11.6 (C29) and 11.5 (C18), and six carbons assignable to sugar moiety at 100.8 (C1'), 76.1 (C5'), 75.5 (C3'), 73.3 (C2'), 69.7 (C4') and 61.4 (C6') (Table 2, Additional file 1: Fig. S11). The DEPT-135 spectrum displayed the presence of 12 methylene signals including one belong to the glucopyranose moiety (Additional file 1: Fig. S12). The spectral data of compound **3** that obtained in this study is found to be in good agreement with previously reported data of *β*-Sitosterol-3-*O*-*β*- D-glucoside [26], Fig. 1, reported herein for the first time from the roots of *H. johannis*.

Antibacterial activity

The in vitro antibacterial activities of *n*-hexane, DCM/MeOH (1:1) and MeOH (100%) extracts from the root of *H. johannis* and isolated compounds **2** and **3** from DCM/MeOH (1:1) were tested against *E. coli*, *S. aureus, P. aeruginosa*, and *S. pyogen* pathogens at concentrations of 0.25, 0.50, and 1.00 mg/mL. The average inhibitory zone diameters (in mm) of the extracts and identified compounds (**2** and **3**) against the growth of each bacterial strain are shown in Tables 3 and 4, respectively. In most cases, the DCM/MeOH (1:1) extract was shown to be more active than the *n*-hexane and MeOH extracts in inhibiting the growth of each of the tested bacterial strains Table 3). At the concentration of 0.25 mg/mL, the

Table 3 Inhibition zone (mean ± SD, in mm) of n-hexane, DCM/MeOH (1:1) and MeOH extracts

Samples	Concentrations (mg/mL)	Bacterial strains			
		E. coli	*P. aeruginosa*	*S. aureus*	*S. pyogen*
n-Hexane	0.25	8.25 ± 0.25	8.5 ± 0.5	9.25 ± 0.25	9.5 ± 0.5
	0.5	10.25 ± 0.25	9.5 ± 0.5	10.5 ± 0.5	11.25 ± 0.25
	1	11.75 ± 0.25	11.5 ± 0.5	12.5 ± 0.5	13.75 ± 0.75
DCM/MeOH	0.25	9.5 ± 0.5	10.5 ± 0.5	10.75 ± 0.25	8.5 ± 0.5
	0.5	11 ± 0.0	12.25 ± 0.25	11.5 ± 0.5	9.5 ± 0.5
	1.0	13.75 ± 0.25	14.25 ± 0.25	13 ± 0.0	11.5 ± 0.5
MeOH	0.25	7.75 ± 0.75	8.00 ± 1.0	8.5 ± 0.0	8.25 ± 0.25
	0.5	9 ± 1.0	9.25 ± 1.25	10 ± 1.0	9.75 ± 0.75
	1.0	10.25 ± 0.5	11.5 ± 1.0	12.25 ± 0.75	11.5 ± 0.5
Amoxicillin (0.25 mg/mL)		15.25 ± 0.25	15.25 ± 0.25	16.0 ± 0.0	16.25 ± 0.25

Table 4 Inhibition zone (mean ± SD, in mm) of isolated compounds **2** and **3**

Conc. (mg/mL)	Compounds	Bacterial strains			
		E. coli	*P. aeruginosa*	*S. aureus*	*S. pyogen*
0.25	2	11.5 ± 0.5	12.0 ± 0.0	10.75 ± 0.25	11.0 ± 0.0
	3	9.0 ± 0.0	10.75 ± 0.25	10.0 ± 0.5	9.5 ± 1.5
0.50	2	12.75 ± 0.75	13.5 ± 0.5	11.75 ± 0.25	12.0 ± 0.0
	3	11.25 ± 0.25	11.75 ± 0.75	11.5 ± 0.5	11.0 ± 0.5
Amoxicillin (0.25 mg/mL)		15.25 ± 0.25	16.0 ± 0.0	15.25 ± 0.25	16.25 ± 0.25

extracts displayed promising growth inhibitory effect against all the selected bacterial strains. The highest inhibition zone was measured for DCM/MeOH extract (10.75 ± 0.25 mm) against *S. aureus*, which is promising in comparison to the standard, amoxicillin (16.0 ± 0.0 mm). In addition, the DCM/MeOH extract exhibited growth inhibition effect against *P. aeruginosa*, *E. coli*, and *S. pyogen*, with mean inhibition zones of 10.5 ± 0.5, 9.5 ± 0.5, and 8.5 ± 0.5 mm, respectively. At the same concentration of 0.25 mg/mL, the n-hexane extract scored maximum mean inhibition zone of 9.5 ± 0.5 mm against *S. pyogen*, followed by 9.25 ± 0.25, 8.5 ± 0.5, and 8.25 ± 0.25 mm against *S. aureus, P. aeruginosa*, and *E. coli*, respectively. The MeOH extract displayed highest inhibitory effect against *S. aureus*, with inhibition zone of 8.5 ± 0.0 mm, and then against *S. pyogen* (8.25 ± 0.25 mm), *P. aeruginosa* (8.00 ± 1.0 mm), and *E. coli* (7.75 ± 0.75 mm). In comparison to the *n*-hexane and MeOH extract, at higher concentration of 1.0 mg/mL) also, DCM/MeOH extract showed the highest mean inhibition zone (14.25 ± 0.25) against *P. aeruginosa*, than against the other studied bacterial strains. Likewise, the n-hexane and MeOH extract showed good antibacterial activity against *S. pyogen* (13.75 ± 0.75, and 12.25 ± 0.75 mm respectively) than the other tested bacterial strains. The result also showed that, at 0.25 mg/mL, all the three extracts (*n*-hexane, DCM/MeOH, and MeOH) showed significant growth inhibition against the gram-positive bacterial strain *S. aureus* (9.25 ± 0.25, 10.75 ± 0.25, and 8.5 ± 0.0 mm), which is considerable compared to the standard drug, amoxicillin (16.0 ± 0.0 mm). The in vitro antibacterial activity result shows that the tested bacterial strains are susceptible to each extract. In a previous study, the MeOH extract of roots of *H. johannis* showed mean inhibitory effects against *E. coli, P. aeruginosa*, and *S. aureus* at mean inhibition zone of in 9 mm, 8 mm, and 8 mm, respectively [7], which is in agreement with the result reported in current study.

The antibacterial activity of compound **1** (*β*-sitosterol) has been studied by many researchers. According to Sileshi and his co-workers, report, *β*-sitosterol found to have low/moderate antibacterial activity against several bacterial species that include *E. coli, S. aureus* and *P. aeruginosa* [24]. Other reports also indicate that the compound demonstrated significant growth inhibition effect against both gram-positive and gram-negative bacterial strains [22, 23]. In this work the in vitro antibacterial of compounds **2** and **3** were reported. Table 4

displayed the mean inhibition zone of isolated compounds **2** and **3** against *E. coli, P. aeruginosa, S. aureus*, and *S. pyogen*. The obtained reported shows that the tested compounds **2** and **3** exhibited growth inhibitory effect against all the tested bacterial strains in a dose dependent manner. At concentration of 0.25 mg/mL, the larger average growth inhibition zone of 12.0 ± 0.0 mm was measured for compound **2** against *P. aeruginosa*, which is good in comparison to the standard drug, amoxicillin (16.0 ± 0.0 mm). Compound **2** also showed the highest antibacterial activity against *E.coli*, *S. pyogen*, and *S. aureus* with average inhibition zone of 11.5 ± 0.5, 11.0 ± 0.0, and 10.75 ± 0.25 mm, respectively. Compound **3** recorded the next largest inhibitory effect against *P. aeruginosa* with inhibition zone of 10.75 ± 0.25 mm, and then against *S. aureus* (10.0 ± 0.5), 9.5 ± 1.5 (*S. pyogen*), and 9.0 ± 0.0 mm (*E. coli*). Similarly, at higher concentration, 0.50 mg/mL, the larger mean inhibition zone of 13.5 ± 0.5 was measured for compound 2 against *P aeruginosa*. Results from previous antibacterial activity study result, using agar diffusion method, showed that compound **3** exhibited mean inhibition zone of 0.9 mm against each *P. aeruginosa* and *S. aureus* at concentration of 0.25 mg/mL [27]. The mean inhibition zone reported for compound **3** in our study is good agreement with the previous one. The overall antibacterial activity result shows, irrespective of their lower antibacterial activities relative to the standard compound (amoxicillin), indicated that compounds **2** and **3** exhibited promising growth inhibitory effect against the tested bacterial strains, which support the use of *H. johannis* in tradition medication system.

Molecular docking studies of the isolated compounds

The molecular docking study was carried out to assess the binding affinity and binding interactions of isolated compounds **1–3** toward target proteins *E.coli* DNA gyrase B (PDB ID 6F86), *S. aureus* PK (PDB ID: 3T07), and PqsA (PDB ID: 5OE3). The binding affinity, H-bond, and residual interaction of all the isolated compounds are summarized in Tables 5, 6 and 7.The docked compounds **1–3** displayed minimum binding energies ranged from − 7.6 to − 6.2 kcal/mol, − 8.7 to − 8.0 kcal/mol, and − 7.4 to − 7.0 kcal/mol, with DNA gyrase, PqsA, and *S. aureus* PK, respectively (Tables 5, 6 and 7). Such low docking score values signify a good interaction of the compounds with protein binding pocket. In the study, each of the isolated compounds (**1–3**) demonstrated better binding affinity (binding energy of − 7.6 to − 6.2 kcal/mol) against protein DNA gyrase than the standard drug, amoxicillin (− 6.1 kcal/mol). The highest binding affinity (− 7.6 kcal/mol) was recorded by compound **2** (− 7.6 kcal/mol) followed by compound **3** (− 6.5 kcal/mol). When docked to the protein PqsA, each compound (**1–3**) displayed higher binding affinities (− 8.7 to − 8.0 kcal/mol) compared to the standard, amoxicillin (− 7.3 kcal/mol). Compound **2** showed the highest binding affinity (− 8.7 kcal/mol), followed by compound **3** (− 8.6 kcal/mol) and compound **1** (− 8.0 kcal/mol). The binding affinities of the ligands (**1–3**) to the protein *S. aureus* PK (− 7.4 to − 7.0 kcal/mol) were found to be equal to or better than amoxicillin (− 7.0 kcal/mol). Of these, the strongest binding affinity was displayed by compound **2** (− 7.4 kcal/mol). In general, at each ligand-protein pose, compound **2** scored the highest binding affinity [− 8.7 kcal/mol (against DNA gyrase), − 7.6 kcal/mol (PqsA), and − 7.4 kcal/mol (*S aureus* PK)]. Compounds **1** and **3** also scored significant binding affinity [DNA gyrase (− 6.2 and − 6.5 kcal/mol), PqsA (− 8.0 and − 8.6 kcal/mol, *S. aureus* PK (− 7.0 kcal/mol each)].

Based on the molecular docking analysis results, the isolated compounds (**1–3**) displayed H-bond, hydrophobic van der Waals interactions with binding pockets of DNA gyrase, PqsA, and *S. aureus* PK (Tables 6, 7 and 8). The amino acid residues that are involved in hydrogen bonds, hydrophobic, and van der Waals interactions at each ligand- protein complexes were also mapped using AutoDock Vina (Figs. 2, 3 and 4, and Tables 6, 7 and 8).The binding affinity of compound **2** with gyraseB (-7.6 kcal/mol) was stabilized by hydrogen bonds at amino acid residues Glu-50, Gly-77 and Ser-121, hydrophobic interaction at Ile-94 and Ile-78, and van der Waals interaction at Arg-76, Pro-79, Gly-75, Asp-73, Thr-165,

Table 5 Docking scores of isolated compounds **1–3** against *E. coli* DNA (PDB ID: 6F86)

Cmpds	Affinity (kcal/mol)	H-bond	Residual interactions	
			Hydrophobic	Van Dar Waals
1	− 6.2	Val-97	Ile-78, Ile-94, Pro-79	Arg-76, Glu-50, Asn-46, Asp-49, Ale-98, Ser-121
2	− 7.6	Glu-50, Gly-77, Ser-121	Ile-94, Ile-78	Arg-76, Pro-79, Gly-75, Asp-73, Thr-165, Gly-164, Asn-46, Gly-117, Val-118, Leu-98, Val-97, Gly-119, Val-120
3	− 6.5	Asn-46, Gly-77, Arg-76	Leu-52, Ala-53, Pro-79	Sp-49, Ile-78, Ile-94, Ala-47, Gly-75
Amox	− 6.1	Arg-76, Asp-49		Asp-73, Ala-47, Ile-78, Asn-46, Ile-94, Pro-79, Gly-75, Gly-164

Table 6 Docking score of isolated compounds **1–3** against *Pseudomonas aerugi*nosa PqsA

Cmpds	Affinity (kcal/mol)	H-bond	Residual interactions	
			Hydrophobic/Pi-sigma/alkly/Pi-alkalyl	Van dar Waals
1	− 8.0	Gly-302	Phe-209, Val-254, Pro-234, Ile-204	Ile-257, pro-205, Lys-206, Trp-233, Gly-279, Tyr-211, Phe-208, Ala-303, Phe-209
2	− 8.7	Pro-85, Lys-86, Ala-108	Ala-124, Leu-60, Arg-128, Ala-108	Arg-106, A: Pro-111, Ala-110, Asp-109, Asn-61, Phe-134, Leu-66, Ser-65, Ala-125, A: Gly-127, Ala-126
3	− 8.6	Gly-279, Asp-282	Val-254, A: Pro-205 A: Ile-204, A; Ile-257, Phe-209	Pro-234, Tyr-211, Phe-208, Trp-233, Gly-210, Ala-303, Gly-302, Arg-397, His-394, Ile-301, Thr-304
Amox	− 7.3	Lys-86, Pro-129, Ala-125	Arg-128, Ala-124, Pro-129	Glu-107, Asp-231, Tyr-25, Ser-63, Pro-64, Leu-130, Ser-65, Asp-132, Ala-126, Gly-127, Thr-232

Gly-164, Asn-46, Gly-117, Val-118, Leu-98, Val-97, Gly-119 and Val-120. The docking of compound **1** and **3** with DNA gyrase stabilized by H-bond, hydrophobic van der Waals interactions across various amino acid residues (Table 5; Fig. 2). At its heavy negative binding energy of − 8.7 kcal/mol with protein PqsA, compound **2** displayed hydrogen bonds with residual amino acids Pro-85, Lys-86, and Ala-108, hydrophobic interaction with Ala-124, Leu-60, Arg-128, and Ala-108, and large number (ten) of Van Dar Waals interaction with Arg-106, Pro-111, Ala-110, Asp-109, Asn-61, Phe-134, Leu-66, Ser-65, Ala-125, A: Gly-127, and Ala-126. Similarly, the low binding energy interactions of compound **1** (− 8.0 kcal/mol) and **3** (− 8.6 kcal/mol) with protein PqsA involved H-bonds, hydrophobic and van der Waals interactions across various residual amino acids at its binding pocket (Table 6; Fig. 3). In its interaction with *S. aurues*PK, compound **2** (binding energy of − 7.4 kcal/mol) displayed seven hydrogen bonds at Glu-234, Leu-233, Ser-236, Asp-237, Lys-271, Asn-357, and Leu-269, which is assumed to boost its binding affinity (Table 7; Fig. 4). Likewise, the docking result revealed that the recorded binding affinities of compound **1** and **3** with the protein *S. aureus* (− 7.0 kcal/mol each) were mediated by hydrogen bond, hydrophobic, and van der Waals interactions that are formed across various amino acids. Overall, the results obtained from the molecular docking study agreed with the in vitro antibacterial activity against *E.coli*, *P. aeruginosa*, and *S. aureus*. The highest binding affinities of compound **2** to DNA gyrase (− 7.6 kcal/mol), PqsA (− 8.7 kcal/mol), and *S. aureus* (− 7.4 kcal/mol) are in agreement with its highest in vitro antibacterial activity result. In addition, at each docking pose, all the tested compounds **(1–3)** scored binding affinities better than the standard amoxicillin. The binding affinity, H-bond and residual amino acid interactions of the three compounds and amoxicillin are summarized in Tables 5, 6 and 7. The mapped binding interactions of compounds **1–3** against targeted proteins are displayed in Figs. 2, 3 and 4. Ribbon model shows the binding pocket structure of target proteins with the compounds. Hydrogen bond between compounds and amino acids are shown as green dash lines, hydrophobic interaction are shown as pink lines.

In silico pharmacokinetic analysis

The *in silico* drug-likeness of the isolated compounds 1–3 was determined based on the concept of Lipinski's rule of five [18] and Veber's rule [28]. Results are given in Table 8. Lipinski's rule of five states that a compound with molecular weight (MW) < 500 Daltons, H-bond donors (NHD) < 5, H-bond, acceptors (NHA) < 10, and a log P of < 5 could be a good drug candidate. Veber's rule says that a compound with rotatable bonds (RTB) < 10 and a polar surface area (TPSA) < 140 ´Å2 should present good oral bioavailability. Compound with a fewer or preferably no violations are likely to be considered as a

Table 7 Docking score of compounds **1–3** against *S. aureus* Pyruvate Kinase

Cmpds	Affinity (kcal/mol)	H-bonds	Residual interactions	
			Hydrophobic	Van dar Waals
1	− 7.0	--	Lys-260	Arg-264, Asp-346, Asp-303, Asp-261, Met-260, Tyr-302, Gly-338
2	− 7.4	Glu-234, Leu-233, Ser-236, Asp-237, Lys-271, Asn-357, Leu-269	Val-356	Arg-204, Val-235, Glu-352, Lys-390, Gly-270,Arg-386
3	− 7.0	Ser-411	Val-419	Glu-440, Val-420, Asp-58, Ile-60, Val-416, B: Lys-5, Gln-417 Thr-441
Amox	− 7.0	Lys-390, Arg-386	Asp-237, Arg-386,Val-356	Asn-357, Thr-387, Ser-383, Lys-271, Ser-381, Ser-215, Pro-272

Table 8 *In silico* pharmacokinetic predictions (drug likeness and ADTE) of isolated compounds **1–3** computed by SwissADME and PreADMET tool

Predicted Parameter	Compounds		
	1	2	3
Drug likeness			
Formula	$C_{29}H_{50}O$	$C_{21}H_{24}O_{11}$	$C_{35}H_{60}O_6$
MW (g/mol)	414.71	452.41	576.85
NHD	1	8	4
NHA	1	11	6
LogP (iLogP)	4.89	1.55	5.29
Lipinski's RO5	Yes	No, 2 violation	No, 1 violation
NRB	6	4	9
TPSA (A°2)	20.23	189.53	99.38
Veber's rule	Yes	No	Yes
ADME predictions			
log Kp cm/s	− 2.69	− 10.08	− 4.32
GIA	Low	Low	Low
BBB	No	No	No
Inhibitory interaction			
P-gp substrate	No	No	No
CYP1A2 inhibitor	No	No	No
CYP2C19 inhibitor	No	No	No
CYP2C9 inhibitor	No	No	No
CYP2D6 inhibitor	No	No	No
CYP3A4 inhibitor	No	No	No

NHD Number of Hydrogen donor, *NHA* Number of Hydrogen acceptor, *NRB* Number of rotatable bonds, *TPSA* total polar surface area, *MW* Molecular weight, *LogKp* Skin permeation value, *GI* Gastro-Intestinal, *BBB* Blood Brain Barrier, *P-gp* P glycoprotein, *CYP* Cytochrome-P.

potential drug candidate. The chemical structures of the compounds (**1–3)** were converted to their corresponding canonical simplified molecular-input line-entry system (SMILE) and submitted to the SwissADME tool to generate the physicochemical and pharmacokinetic properties of the compounds. The SwissADME prediction outcome showed that compound **1** satisfies the Lipinski's rule of five with zero violations. As shown in Table 8, the computed molecular weights for compounds **1** and **2** are found to be asper the rule of five (< 500 g/mol). The NHD and NHA for compounds **1** and **3** were predicted to be according to the Lipinski's rule of five. According to the obtained result, compound **2** obey the MW (< 500 g/mol) and iLogP (1.55) rules, and compound **3** obey the NHD and NHA rules. The LogP value is a significant descriptor for the affinity of molecules to a lipophilic environment [29]. Compounds **2** recorded iLogP value less enough than five (1.55), implying its optimal lipophilicity. The prediction result showed that compound **1** and **3** obeyed the Veber's rule (NRB < 12, and TPSA < 140 unit). Veber's rule says that a compound with 10 or fewer rotatable bonds (NRB) and a polar surface area (TPSA) no greater than 140 ´Å2 should present good oral bioavailability. The total polar surface area (TPSA) value is sufficiently below the cut-off value (140 2 $Å^2$) for compounds **1** and **3** (20.23 and 99.38, respectively), indicating very good absorption by the gut. Our prediction results regarding the drug-like features indicated that Lipinski's rule is obeyed by compound **1** with zero violation. Compound **2** and **3** obeyed the rule of MW and LogP, and NHD and NHA, respectively. Veber's rule is valid for compound **1** and **3**. The ADME properties of compounds **1–3** were performed using the SwissADME tool [17].

The main ADME parameters concerning pharmacokinetic behavior of the tested compounds are presented in Table 9. The logKp (with Kp in cm/s) values of compounds **1–3** were predicted to be -2.69, -10.04 and − 4.32 cm/s, respectively, inferring low skin permeability of each. The more negative the logKp value, the lesser skin permeant the molecule [17]. Compound **2** scored the most negative LogKp value of -10.04 cm/s, indicating its lowest skin permeability compared to other isolated compounds (**1** & **3**). The ADME prediction outcome displayed that, all tested compounds (**1–3**) were found to be non-substrate of permeability glycoprotein (P-gp), and hence non-inhibitors of all the selected cytochromes (CYP1A2, CYP2C19, CYP2C9, CYP2D6, and CYP3A4).

The toxicity profiles of the studied compound were carried out using ProTox II. The predicted toxicity results of

Table 9 Prediction of Toxicity of isolated compounds **1–3** computed by ProTox-II.

Compounds	LD_{50} (mg/Kg)	Toxicity class	Organ toxicity				
			Hepato	Carcino	Immuno	Mutagen	Cyto
1	890	4	Inactive	Inactive	Active	Inactive	Inactive
2	10,000	6	Inactive	Inactive	Inactive	Inactive	Inactive
3	8000	6	Inactive	Inactive	Active	Inactive	Inactive

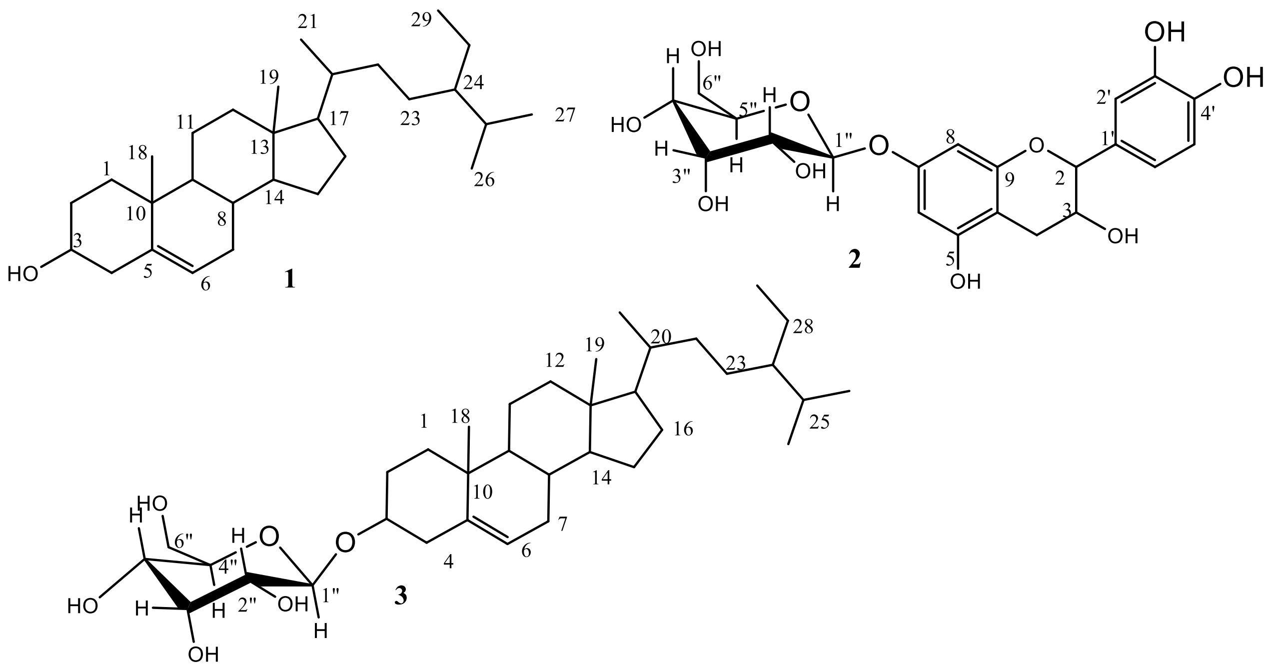

Fig. 1 Structures of compounds (**1–3**) isolated from the root of *H. johannis*

the studied compounds (**1–3**) were presented in Table 9. Compound **2** and **3** exhibited negligible acute toxicity (LD50 > 5000, Toxicity class > 5). The ProTox-II prediction also gives toxicological endpoints such as hepatotoxicity, carcinogenicity, immunotoxicity, mutagenicity and cytotoxicity results. Hepatotoxicity predictions indicate that all studied compounds (**1–3**) are unlikely to disturb the liver normal function. The studied compounds **1–3** also exhibited no carcinogenicity, mutagenicity, and cytotoxicity. Compound **2** and **3** have shown immunotoxicity. Based on the reported ADMET prediction analysis, the studied compounds can be good drug candidates, with partial or complete structural modifications.

Radical scavenging activity

The radical scavenging activity of compound **1–3** isolated from the root extract of *H. johannis* were evaluated using the DPPH assay, a simple method to evaluate antioxidant activities by measuring absorbance at 517 nm due to the formation of stable DPPH radical [21]. At all the tested concentrations of each compound, the purple color of the DPPH solution was changed to yellow color indicating potential radical scavenger activity of the compounds. The absorbance of the DPPH radical at 517 nm was also reduced. The DPPH assay result indicated that the compounds showed radical scavenging activity in dose-dependent manner (Table 10). The scavenging activity result evident that of the studied compounds (**1–3**) showed promising radical scavenging activities at all tested concentrations. At the lowest tested concentration of 12.5 µg/mL, the strongest DPPH scavenging activity was recorded by compound **2** (67.87%), with IC_{50} value of 0.190 µg/mL, which is in good comparison to the standard, ascorbic acid (78.21%), with IC_{50} value of 0.014 µg/mL. Compound **1** and **3** also showed considerable percentage

Table 10 DPPH radical inhibition of isolated compounds **1–3**

	200 µg/mL	100 µg/mL	50 µg/mL	25 µg/mL	12.5 µg/mL	
1	61.44 ± 0.3	57.47 ± 0.1	56.43 ± 0.01	51.16 ± 0.25	49.76 ± 0.66	14.668
2	79.74 ± 0.04	77.36 ± 0.02	75.03 ± 0.01	70.99 ± 0.1	67.87 ± 0.02	0.190
3	67.07 ± 0.01	65.48 ± 0.01	61.44 ± 0.03	57.77 ± 0.02	52.75 ± 0.01	6.250
Asc acid	90.51 ± 0.03	82.19 ± 0.03	80.17 ± 0.02	79.50 ± 0.02	78.21 ± 0.03	0.014

Samples were reported as Mean ± SD; Ascorbic acid was used as positive control

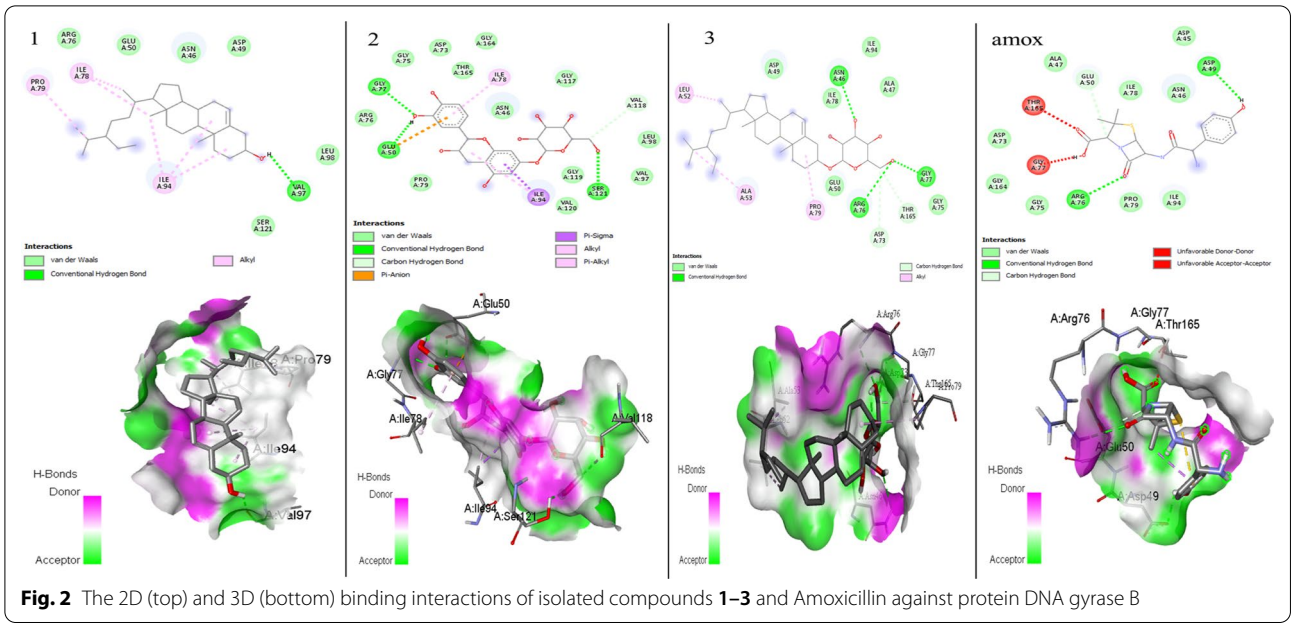

Fig. 2 The 2D (top) and 3D (bottom) binding interactions of isolated compounds **1–3** and Amoxicillin against protein DNA gyrase B

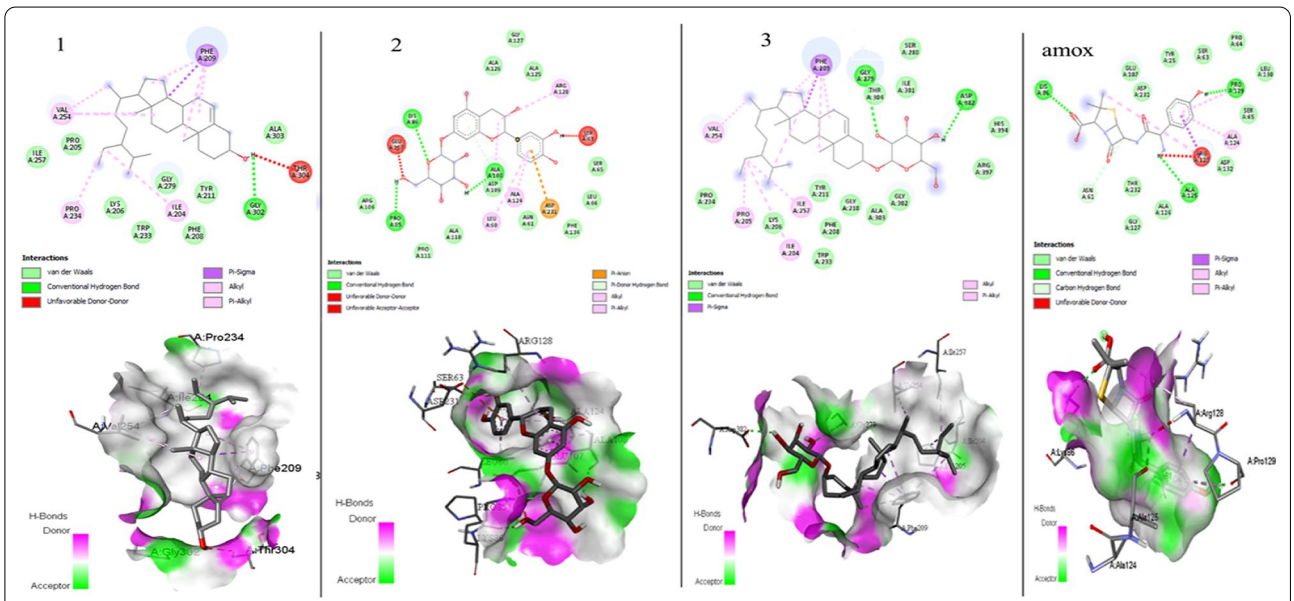

Fig. 3 2D (top) and 3D (bottom) binding interaction of isolated compounds **1–3** and Amoxicillin against protein *P. aeruginosa* PqsA

scavenging activity (52.75%, and 49.76%), with IC_{50} value of 6.250 and 14.668 µg/mL, respectively, which is lower in comparison to the standard. The strongest DPPH scavenging activity of compound **2** compared to other tested compounds, which is good compared ascorbic acid, in this report can be justified due to its proton-donating ability (Fig. 1), which make it to have higher NHD and NHA reported in the drag likeness in this study. Overall, the radical scavenging activity results of the studied compounds are consistent with the drug likeness predictions outcomes.

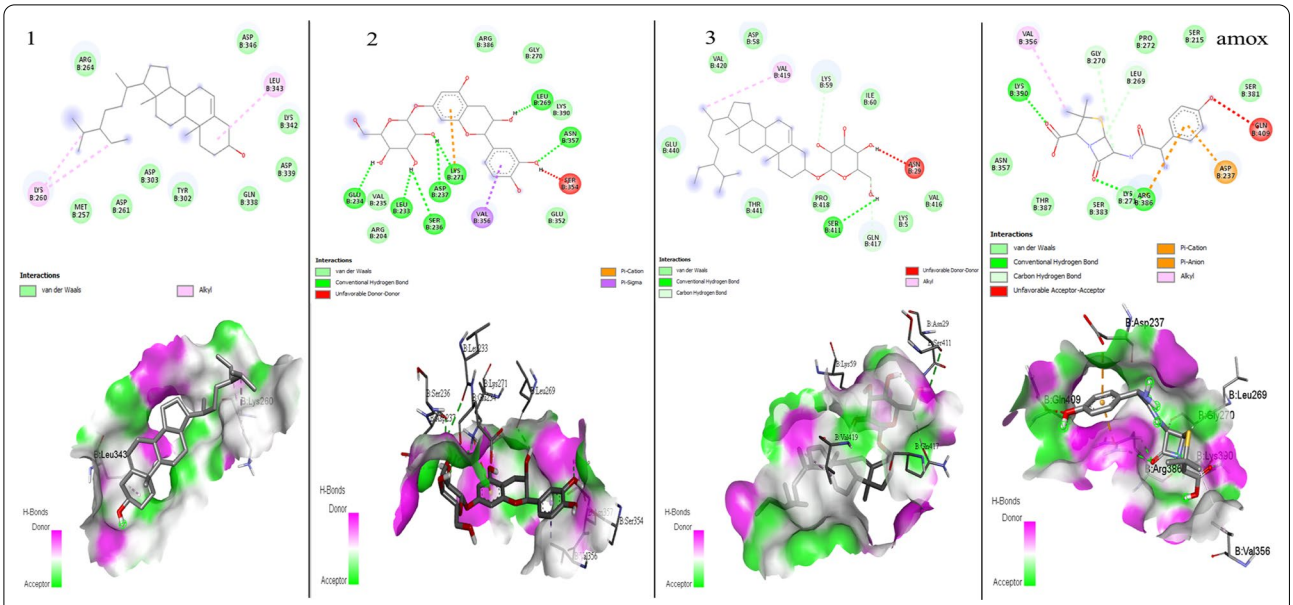

Fig. 4 2D (top) and 3D (bottom) binding interaction of isolated compounds **1–3** and Amoxicillin against protein *S. aureus* PK.

Supplementary Information

The online version contains supplementary material available at https://doi.org/10.1186/s13765-022-00740-8.

Additional file 1: Table S-1. 1H, 13C, HMBC spectral data of compound **2**. **Fig. S1**. 1H NMR spectra of compound **1**. **Fig. S2**. 13C NMR spectra of compound **1**. **Fig. S3**. DEPT-135 spectra of compound **1**. **Fig. S4**. 1H NMR spectra of compound **2**. **Fig. S5**. 13C NMR spectra of compound **2**. **Fig. S6**. DEPT-135 spectra of compound **2**. **Fig. S7**. COSY spectra of compound **2**. **Fig. S8**. HSQC spectra of compound **2**. **Fig. S9**. HMBC spectra of compound **2**. **Fig. S10**. 1H NMR spectra of compound **3**. **Fig. S11**. 13C spectra of compound **3**. **Fig. S12**. DEPT-135 spectra of compound **3**. **Fig. S13**. Photo of Hydnora johannis. (Source: Photo taken by Teshoem Degfie).

Acknowledgements

We thank Adama Science and Technology University for the research fund with grant number: ASTU/AS-R/003/2020. We are also grateful to the World Academy of Sciences (TWAS) and the United Nations Educational, Scientific and Cultural Organization (UNESCO) for financing this research with funds allocated to the AD research team under the TWAS Research Grant RGA No. 20–274 RG/CHE/AF/AC-G - FR3240314163.

Author contributions

AD and ME designed the experiments. TD conducted the isolation, biological activity assay and elucidation the structures. TT conducted molecular docking studies. KS assisted the laboratory work for isolation. TD, AD and ME revised interpreted the data and prepared the paper. AD, ME and TD revised the manuscript. All authors read and approved the final manuscript.

Funding

Adama Science and Technology University for the research fund with grant number: ASTU/AS-R/003/2020. The World Academy of Sciences (TWAS) Research Grant RGA No. 20–274 RG/CHE/AF/AC-G-FR3240314163.

Availability of data and materials

All data generated or analyzed during this study are included in this published article.

Declarations

Ethics approval and consent to participate

Not applicable.

Competing interests

There is no conflict of interests.

Received: 13 July 2022 Accepted: 24 October 2022
Published online: 16 November 2022

References

1. Thorogood C (2019) *Hydnora*: the strangest plant in the world ? Plants. People Planet 1(1):5–7
2. Musselman LJ, Visser JH (1989) Taxonomy and natural history of *Hydnora* (Hydnoraceae). Aliso: J Syst Flor Bot 12(2):317–326
3. Yagi S, Chrétien F, Duval RE, Fontanay S, Maldini M, Piacente S, Henry M, Chapleur Y, Laurain-Mattar D (2012) Antibacterial activity, cytotoxicity and chemical constituents of *Hydnora johannis* roots. S Afr J Bot 78:228–234
4. Musa MS, Abdelrasool FE, Elsheikh EA, Ahmed LAMN, Mahmoud ALE, Yagi SM (2011) Ethnobotanical study of medicinal plants in the Blue Nile State, South-eastern Sudan. J Med Plants Res 5:4287–4297
5. Yagi S, Drouart N, Bourgaud F, Henry M, Chapleur Y, Laurain-mattar D (2013) Antoxidant and antiglycation properties of *Hydnora johannis* roots. S Afr J Bot 84:124–127
6. Al-Fatimi M, Ali NA, Kilian N, Franke K, Arnold N, Kuhnt C, Schmidt J, Lindequist U (2016) Ethnobotany, chemical constituents and biological activities of the flowers of *Hydnora abyssinica* A. Br. (Hydnoraceae). Die Pharm Int J Pharm Sci 71(4):222–226
7. Saadabi AMA, Ayoub SMH (2009) Comparative bioactivity of *Hydnora abyssinica* A. Braun against different groups of fungi and bacteria. J Med Plants Res 3:262–265
8. Nethathe BB, Ndip RN (2011) Bioactivity of *Hydnora africana* on selected bacterial pathogens: preliminary phytochemical screening. Afr J Microbiol Res 5:2820–2826
9. Dagne E (2016) Species details http://www.alnapnetwork.com/SpeciesDetail.aspx SEARCH. http://www.alnapnetwork.com/SpeciesDetail.aspx. Accessed 17 Sep 2022

10. Bussa NF, Belayneh A (2019) Traditional medicinal plants used to treat cancer, tumors and inflammatory ailments in Harari Region, Eastern Ethiopia. S Afr J Bot 122:360–368
11. Girma B, Mulisa E, Amelo W (2018) Ethnomedicine claim activity directed in silico prediction of anticancer. Ethiop J Heal Sci 28:83–92
12. Belayneh A, Asfaw Z, Demissew S, Bussa NF (2012) Medicinal plants potential and use by pastoral and agro-pastoral communities in Erer Valley of Babile Wereda, Eastern Ethiopia. J Ethnobiol Ethnomed 8:1–11
13. Balouiri M, Sadiki M, Ibnsouda SK (2016) Methods for *in vitro* evaluating antimicrobial activity: a review. J Pharm Anal 6:71–79
14. Zaidan MR, Noor Rain A, Badrul AR, Adlin A, Norazah A, Zakiah I (2005) *In vitro* screening of five local medicinal plants for antibacterial activity using disc diffusion method. Trop Biomed 22:165–170
15. Trott O, Olson AJ (2009) AutoDock Vina: Improving the speed and accuracy of docking with a new scoring function, efficient optimization, and multithreading. J Comput Chem 31:455–461
16. Narramore S, Stevenson CEM, Maxwell A, Lawson DM, Fishwick CWG (2019) New insights into the binding mode of pyridine-3-carboxamide inhibitors of *E. coli* DNA gyrase. Bioorg Med Chem 27:3546–3550
17. Daina A, Michielin O, Zoete V (2017) SwissADME: a free web tool to evaluate pharmacokinetics, drug-likeness and medicinal chemistry friendliness of small molecules. Sci Rep 7(1):1–13
18. Lipinski's CA, Dominy BW, Feeney PJ, (2012) Experimental and computational approaches to estimate solubility and permeability in drug discovery and development settings. Acta Petrol Sin 28:1765–1784
19. Banerjee P, Eckert AO, Schrey AK, Preissner R (2018) ProTox-II: A webserver for the prediction of toxicity of chemicals. Nucleic Acids Res 46(W1):W257–W263
20. Behrouz S, Soltani Rad MN, Taghavi Shahraki B, Fathalipour M, Behrouz M, Mirkhani H (2019) Design, synthesis, and in silico studies of novel eugenyloxy propanol azole derivatives having potent antinociceptive activity and evaluation of their β-adrenoceptor blocking property. Mol Divers 23:147–164
21. Gülçin I (2010) Antioxidant properties of resveratrol: a structure-activity insight. Innov Food Sci Emerg Technol 11:210–218
22. Pierre Luhata L, Usuki T (2021) Antibacterial activity of β-sitosterol isolated from the leaves of *Odontonema strictum* (Acanthaceae). Bioorg Med Chem Lett 48:128248
23. Ododo MM, Choudhury MK, Dekebo AH (2016) Structure elucidation of β-sitosterol with antibacterial activity from the root bark of *Malva parviflora*. Springerplus 5:1–11
24. Sileshi W, Adane L, Tariku Y, Muleta D, Begashaw T (2012) Evaluation of antibacterial activities of compounds isolated from *Sida*. Nat Prod Chem Res 1:1–8
25. Friedrich W, Galensa R (2002) Identification of a new flavanol glucoside from barley (*Hordeum vulgare* L.) and malt. Eur Food Res Technol 214:388–393
26. Peshin T, Kar HK (2017) Isolation and characterization of β-sitosterol-3-O-β-D-glucoside from the extract of the flowers of *Viola odorata*. Br J Pharm Res 16:1–8
27. Wong KC, Hag Ali DM, Boey PL (2012) Chemical constituents and antibacterial activity of *Melastoma malabathricum* L. Nat Prod Res 26:609–618
28. Veber DF, Johnson SR, Cheng HY, Smith BR, Ward KW, Kopple KD (2002) Molecular properties that influence the oral bioavailability of drug candidates. J Med Chem 45:2615–2623
29. Daina A, Zoete V (2016) A boiled-egg to predict gastrointestinal absorption and brain penetration of small molecules. Chem Med Chem 11:1117–1121

Publisher's Note